Physica Scripta

PAPER

Assessment of structural, physical properties as well as radiation safety competence of lithium borate glass-ceramics: Experimental and theoretical evaluation

RECEIVED
22 December 2022

REVISED
19 February 2023

ACCEPTED FOR PUBLICATION
24 February 2023

PUBLISHED
7 March 2023

Neslihan Ekinci[1], **Norah A M Alsaif**[2], **Bunyamin Aygün**[3], **Sevda Sarıtaş**[1], **Sedanur Kalecik**[1] and **Y S Rammah**[4]

[1] Department of Physics, Faculty of Sciences, Atatürk University, 25240, Erzurum, Turkey
[2] Department of Physics, College of Science, Princess Nourah bint Abdulrahman University, Riyadh, Saudi Arabia
[3] Department of Physics, Faculty of Sciences, Ağrı İbrahim Çeçen University, Ağrı, Turkey
[4] Department of Physics, Faculty of Science, Menoufia University, Shebin El-Koom 32511, Menoufia, Egypt

E-mail: dr_yasser1974@yahoo.com (**Y. S. Rammah**)

Keywords: lithium tetraborate, XRD, radiation shielding, HVL, EpiXS software

Abstract

Samples of lithium borate glass-ceramics with a composition of $40Li_2B_4O_7 + xBi_2O_3 + (55\text{-}x)\ ZrO_4 + 5CaWO_4$ (x = 10–50 wt%) have been fabricated via ordinary melt quenching route. The physical and structural features have been investigated. Radiation shielding competence has been examined experimentally using an Ultra Ge detector with the ^{133}Ba (3 Ci) radioisotope source and theoretically via EpiXS software. X-ray diffraction showed that the structure of the B1 sample has large crystal particle sizes. However, the structure with the smallest amount of ZrO_4 and the largest amount of Bi_2O_3 has become completely amorphous (sample B5). The density of the synthesized samples were noticed to change between 4.70 to 5.99 g cm^{-3} for B1 and B5 samples, respectively. The B5 sample with high density possessed the highest mass attenuation coefficient (MAC) among other samples. There is an agreement between experimental and theoretical data. The trend of the linear attenuation coefficient (LAC) is the same as that of the MAC. At any certain energy, the half-value layer (HVL) is arranged as; $(HVL)_{B5} > (T_{1/2})_{B4} > (T_{1/2})_{B3} > (T_{1/2})_{B2} > (T_{1/2})_{B1}$. The mean free path (MFP) of the investigated samples is similar to that of the HVL. The recommended glass ceramics can be used as radiation shielding materials.

1. Introduction

Using of high-energy ionizing radiation, particularly gamma-rays is expanding quickly in many areas such as industry, medical diagnostics, nuclear experiment facilities, and biological studies [1]. Today, several safety measures can be taken to protect against the harmful influences of radiation. Radiation protection can be achieved in essentially four different ways, decreasing the source's intensity, expanding the distance, shortening the exposure time, and radiation shielding.

Radiation shielding is the most important of the precautions listed above. Because the only way to lower radiation exposures to acceptable low levels after the first three parameters are fixed is to use radiation shielding. As is known, the shield is a term used to describe materials designed to reduce radiation intensity. Radiation shielding is the process of preventing the penetration or reducing the dose of radiation absorbed by placing an absorber material between a person, a work area, or a radiation-sensitive device and any radioactive source. Materials to be prepared for use in the shielding process are manufactured as a result of a meticulous study, taking into account the characteristics such as the type of beam, intensity, power, and impact area of the radioactive source used. At the same time, the weight, area, cost, and attenuation properties of the material used for radioactive shielding are key factors that make it difficult for researchers to synthesize suitable shielding materials. Lead [2], brick, heavy aggregate concrete, steel, polymers [3], alloys [4], and glass [5–15] are among the materials utilized in the fabrication of the radiation shielding material. However, lead, one of these radiation-

© 2023 IOP Publishing Ltd

Table 1. Samples code, chemical compositions (wt %), and density of the prepared B1-B5 glasses.

	B1	B2	B3	B4	B5
Density (g/cm^3)	4.70	5.03	5.35	5.64	5.99
$Li_2B_4O_7$	40	40	40	40	40
Bi_2O_3	10	20	30	40	50
ZrO_4	45	35	25	15	5
$CaWO_4$	5	5	5	5	5

shielding materials, can be considered advantageous due to its high density. However, due to the fine particles that have accumulated on the surfaces of lead items, these materials are poisonous and a health risk. Physical characteristics like hardness and strength are further drawbacks. In this case, lead can pose a problem as gamma radiation shielding. Likewise, the moisture change in concrete is a disadvantage in preferring the use of concrete as a radiation protection material.

Glasses have recently become the most popular of these materials [16–21]. Thanks to their special formulas, the produced radiation shielding glasses offer clear vision thanks to their reliable protection against X-rays and gamma-rays and high light transmittance. These radiation shielding glasses are used in hospitals, X-ray rooms, operating rooms, radiology centers, computerized tomography, angiography laboratories, and health centers such as nuclear medicine. In industry, X-ray quality control, Non-Destructive Testing (NDT), and research laboratories also use them. While providing protection, on the other hand, it can provide a clear vision to the operator.

Recently, the increase in the use of radiation-shielding glasses has led researchers to produce quality radiation-shielding glasses and to further develop the physical properties of these glasses [7–9]. The physical and γ-ray attenuation features of the glass samples developed in this article were investigated experimentally and theoretically. Radiation shielding parameters such as density, hardness, linear- and mass- attenuation coefficients, effective atomic and electron number, relaxation length, half-value layer and tenth-value layer, energy absorption and exposure buildup factors, and an equivalent atomic number have been established both experimentally and theoretically [5–8, 11–19].

The goal of the presented work is devoted to the investigation of the structural and physical characteristics of the synthesized new glassy samples of $Li_2B_4O_7 + Bi_2O_3 + ZrO_4 + CaWO_4$. Radiation safety parameters of the prepared samples are examined experimentally using an Ultra Ge detector with the ^{133}Ba (3 Ci) radioisotope source and theoretically via EpiXS software.

2. Experimental work

2.1. Sample preparation

Utilizing the melt quenching procedure, a new glass system with the following chemical composition was created: $40Li_2B_4O_7 + xBi_2O_3 + (55\text{-}x)ZrO_4 + 5CaWO_4$:x = 10, 20, 30, 40, and 50 weight percent as shown in table 1. The produced mineral mixture was homogeneously mixed using a mixer for 20 min to create glass samples. This mixture was then put in a platinum crucible and heated for 30 min in an electric furnace at 1000 °C to create a homogeneous melt. Then, this melt was put into molds for the platinum plate with a 3.7 cm diameter and 3.6 mm thickness. A photo of the synthesized B1, B2, B3, B4, and B5, in addition lithium tetraborate ($Li_2B_4O_7$) samples is shown in figure 1.

X-ray diffraction pattern (XRD) recorded with Philips (model PW-1729) X-ray tube adopting Cu Kα radiation utilizing a wavelength 1.54nm, step size 0.02 °C; time per step: 21 sec. So, the structural state of the fabricated samples can be analyzed.

2.2. Experimental assessment of radiation shielding parameters

Gamma transmittance measurements were made to investigate the γ-ray attenuation properties of the prepared glasses. The mass- attenuation coefficient (MAC, μ_ρ) and linear attenuation coefficient (LAC, μ) at seven different γ-energies were assigned using the ^{133}Ba (3 Ci) radioisotope source and an Ultra Ge detector (Canberra, 5.9 keV, ~182 eV resolution, operating voltage −1500 V). This action has been achieved through the experimental geometry which is shown in figure 2. Spectra were produced by irradiating samples with γ-photons at energies 53.16, 79.61, 81.00, 276.40, 302.85, 356.01, and 383.85 keV. The spectrum acquisition time for glass samples was 10 min. In order to reduce the statistical errors, measurements were repeated three times. Program Origin 2021 was used to plot the data and measurements were made both with and without the sample of the areas under the peaks corresponding to the pertinent energy. By applying Lambert-rule Beer's [22]:

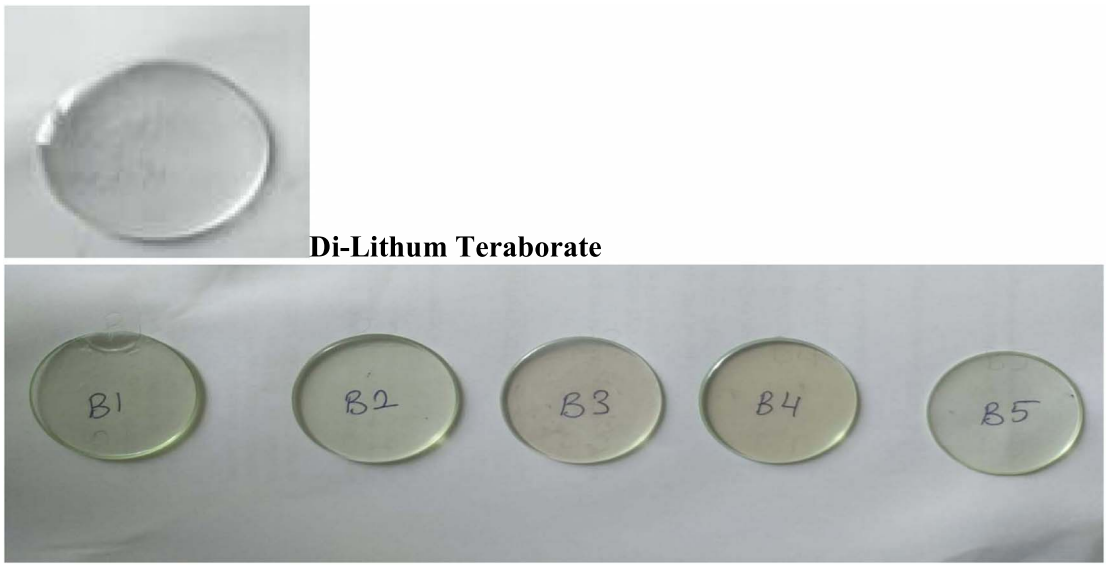

Figure 1. A photo of B1, B2, B3, B4, B5 and lithium tetraborate samples.

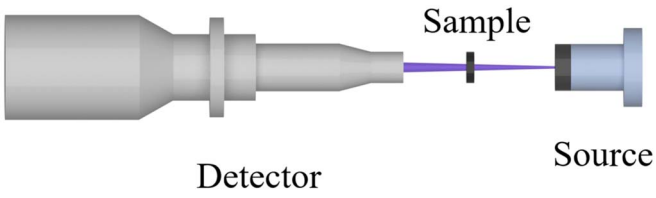

Figure 2. The experimental geometry setup.

$$I = I_o e^{-\mu t} \tag{1}$$

where t is the glass's thickness, and I and I_0 are the glass's primary and transmitted radiation intensities, respectively, the glasses' linear-attenuation coefficient (μ) can be evaluated. By dividing LAC by the material density, one can determine the (μ_ρ) as:

$$\mu_\rho = \frac{\mu}{\rho} = \frac{\ln(I/I_o)}{t\rho} \tag{2}$$

The EpiXS program [23], MCNPX simulation algorithms [24], Phy-X/PSD [25], and XCOM [26] were used to construct the theoretical MAC values after receiving the experimental MAC values in the photon energy range 53–383 keV.

3. Results and discussion

3.1. XRD analysis

XRD measurements should be done to check the structural properties of crystalline materials. XRD is one of the microstructural analysis methods used for the determination of crystallinity of specially doped materials, identification of crystalline phases, and orientation of these materials. The peak intensities and the maximum value of β is the full width at the half in the XRD graph providing information about the quality of the crystal structure. XRD patterns of lithium tetraborate $Li_2B_4O_7$ and B1, B2, B3, B4, and B5 samples are shown in figure 3. With the addition of the $Li_2B_4O_7$ structure to the SiO_2 structure, the amorphous glass structure tried to form broad peaks towards the Lithium Silicon Oxide and Silicon Boron Oxide (Reference code: 01-085-2267) structure to form a crystal structure, as can be understood from XRD. However, a complete crystal structure has not been formed. The peak intensities and the maximum value of β provide information about the quality of the crystal structure. In the B1 structure, where the amount of Bi_2O_3 is a minimum and the amount of ZrO_4 is a maximum, structures with large crystal particle sizes have been formed. However, the B3 structure has the largest average crystalline particle size and the structure with the smallest amount of ZrO_4 and the largest

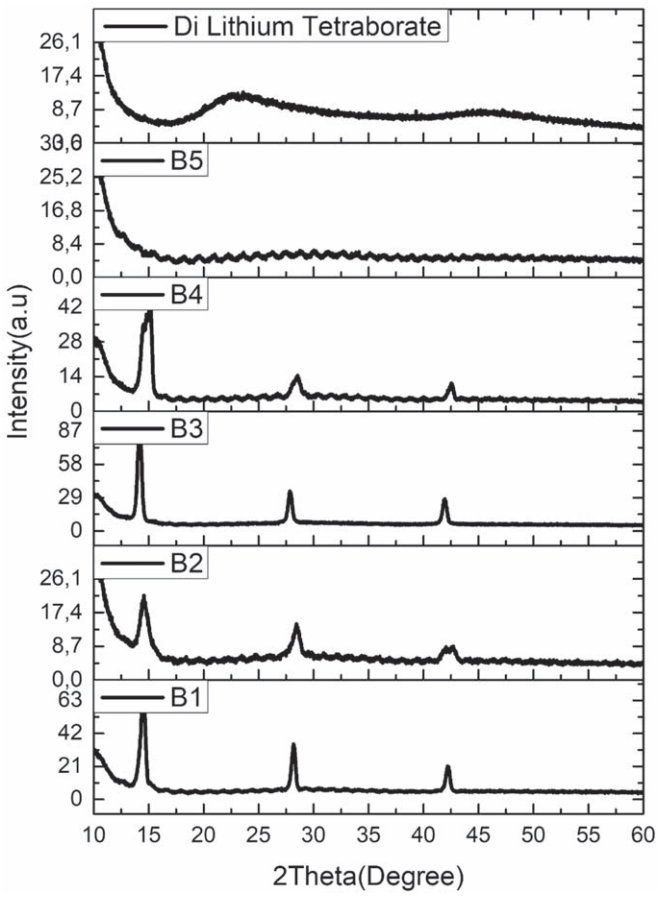

Figure 3. XRD patterns of B1,B2,B3,B4,B5 and lithium tetraborate samples.

amount of Bi_2O_3 has become completely amorphous. This doping in the structure has disrupted the crystal structure of the structure. While the increase in the amount of Bi_2O_3 in the structure resulted in a positive result up to a value, the increase in the ZrO_4 structure in the structure deteriorated the crystal structure. Structures such as bismuth silicon oxide (Reference code: 01-080-0627), $Li_6B_4O_9$ (Reference code:00-018-0721), lithium zirconium oxide (Reference code: 00-041-0324) have been formed in B1, B2, B3, B4, and B5 samples. The grain size of samples was estimated from the XRD pattern via the Debye–Scherrer formula:

$$D = 0.9\lambda/\beta \cos\theta \tag{3}$$

where $\lambda = 1.54$ Å. The estimated crystallite size corresponding to each composition is given in table 2.

3.2. EDXRF analysis

The geometry in which the experimental measurements were carried out is given in figure 2. The representative spectrum obtained when there is no glass sample between the Ultra Ge detector and the Ba-133 source and there is a B1 glass sample in between is shown in figure 4. In the spectrum, the peaks of gamma photons with energies of 53.16, 79.61, 81.00, 276.40, 302.85, 356.01, and 383.85 keV emitted from Ba-133 source are seen. In the representative spectrum in figure 4, it is observed that the B1 glass sample absorbs radiation better at low photon energies of 53.16, 79.61 and 81.00 keV compared to higher energies such as 276.40, 302.85, 356.01 and 383.85 keV.

3.3. Gamma-ray shielding competence

Mass absorption coefficients (MACs) of all samples were obtained experimentally at γ-energies between 81.00 and 383.85 keV using a Ba-133 source. At the same time, the mass absorption coefficients were calculated theoretically in a wide energy scale between 30.8 and 384 keV by the EpiXS program. The comparison between the experimentally measured MACs for the B1-B5 glass samples and the MACs calculated theoretically via the EpiXS software are given in table 3. In addition, the profile of MACs with wide energy scales for each glass sample is plotted in figure 5. The results from figure 5 and table 3 show that there is a net reduction in the overall behavior of MACs with increasing energy as expected, and also a net increase with the addition of larger amounts

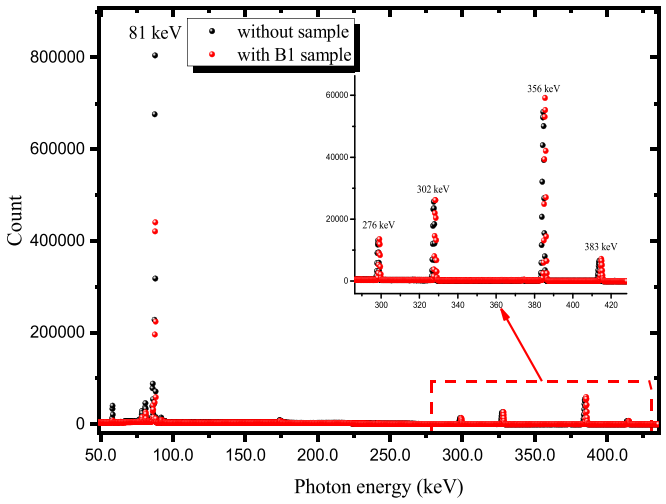

Figure 4. EDXRF of B1 sample at 81 keV.

Table 2. The grain size and FWHM of the B1, B2, B3, B4 and B5 samples.

Samples code	2Theta (Deg.)	FWHM	Intensity	Crystal size (nm)
B1	14,48	0,513	57,26	15,62
	28,18	0,406	27,81	20,19
	42,21	0,422	15,21	20,19
B2	14,57	0,943	12,69	8,490
	28,43	0,691	6,700	11,87
	42,31	2,189	6,582	3,890
B3	14,18	0,431	81,50	18,50
	27,87	0,414	25,24	19,70
	41,92	0,440	20,17	19,10
B4	14,84	1,000	35,33	8,010
	28,43	0,895	7,407	9,160
	42,49	0,522	5,893	16,33
B5	**Amorphous**			

of Bi_2O_3. It is seen that the B5 sample possessed the highest MAC value and the B1 sample possessed the least MAC value. Essentially, these changes in MAC values are related to different photon interaction processes. This according to the photoelectric effect (PE) cross section is directly proportional with Z^{4-5} and $E^{-3.5}$ in the low energy zone (<0.2 MeV) [27, 28]. Hence, the MAC has its highest values at low photon energies and rapidly decreases as photon energy is increased. The Compton scattering (CS) mechanism states that after the sharp decline in the low energy region, the MAC values nearly remain constant at energies greater than 0.15–0.2 MeV. In addition, the relative difference between the experimental and theoretical mass- attenuation coefficients (MACs) is given in table 3, it was in the range of 0.002–0.017 for B1, 0.004–0.015 for B2, 0.004–0.028 for B3, 0.004–0.019 for B4 and 0.003–0.026 for B5. Therefore, the MAC values obey $(MAC)_{B1} < (MAC)_{B2} < (MAC)_{B3} < (MAC)_{B4} < (MAC)_{B5}$.

Another finding is that the LAC values of the B1-B5 glass samples show similar results to the MAC values. Values of LAC of the investigated samples are given in table 4 and plotted in figure 6. The LAC value decreases as increasing of energy and reducing in the amount of Bi_2O_3 added to the glasses. From these results, the B5 glass sample has the best attenuation of gamma rays compared to the prepared B1-B4 samples.

According to the relation ($HVL = \ln 2/LAC$), the HVL can be estimated directly from the LAC values. The changing of HVL for B1-B5 samples with the selected γ- energies is shown in table 5 and figure 7. The HVL arranged as; $(HVL)_{B5} > (T_{1/2})_{B4} > (T_{1/2})_{B3} > (T_{1/2})_{B2} > (T_{1/2})_{B1}$. Furthermore, at 0.384 MeV, the HVL was found 1.271, 1.061, 0.901, 0.779, and 0.674 cm at 0.0308 MeV it was found 0.015, 0.013, 0.011, 0.009, and 0.008 cm for B1, B2, B3, B4 and B5, respectively. Therefore the suggested glass sample B5 can be considered as superior for γ-ray among all investigated samples. Table 6 and figure 8 illustrate the changing of the mean free path (MFP)

Table 3. Theoretical and experimental mass attenuation coefficient (MAC) of B1-B5 samples.

Energy (MeV)	B1 (Theo.) (cm^2/g)	B1 (Exp.) (cm^2/g)	Rel. Diff	B2 (Theo.) (cm^2/g)	B2 (Exp.) (cm^2/g)	Rel. Diff.	B3 (Theo.) (cm^2/g)	B3 (Exp.) (cm^2/g)	Rel. Diff	B4 (Theo.) (cm^2/g)	B4 (Exp.) (cm^2/g)	Rel. Diff	B5 (Theo.) (cm^2/g)	B5 (Exp.) (cm^2/g)	Rel. Diff
3.08E-02	9.646			10.912			12.178			13.444			14.709		
3.50E-02	6.896			7.818			8.739			9.661			10.583		
3.54E-02	6.692			7.588			8.485			9.381			10.277		
3.58E-02	6.497			7.369			8.240			9.112			9.984		
4.96E-02	2.758			3.147			3.537			3.926			4.315		
5.32E-02	2.307			2.635			2.963			3.292			3.620		
8.10E-02	**1.002**	**1.004**	0.002	**1.118**	**1.122**	0.004	**1.234**	**1.229**	0.004	**1.351**	**1.356**	0.004	**1.467**	**1.472**	0.003
1.61E-01	0.368			0.502			0.636			0.771			0.905		
2.23E-01	0.213			0.269			0.326			0.383			0.439		
2.76E-01	**0.161**	**0.165**	0.025	**0.194**	**0.198**	0.021	**0.226**	**0.230**	0.018	**0.259**	**0.261**	0.008	**0.291**	**0.294**	0.010
3.03E-01	**0.145**	**0.151**	0.041	**0.171**	**0.168**	0.018	**0.197**	**0.202**	0.025	**0.222**	**0.218**	0.018	**0.248**	**0.252**	0.016
3.56E-01	**0.124**	**0.129**	0.040	**0.141**	**0.148**	0.049	**0.158**	**0.163**	0.031	**0.175**	**0.179**	0.023	**0.192**	**0.197**	0.026
3.84E-01	**0.116**	**0.114**	0.017	**0.130**	**0.128**	0.015	**0.144**	**0.148**	0.028	**0.158**	**0.161**	0.019	**0.172**	**0.170**	0.012

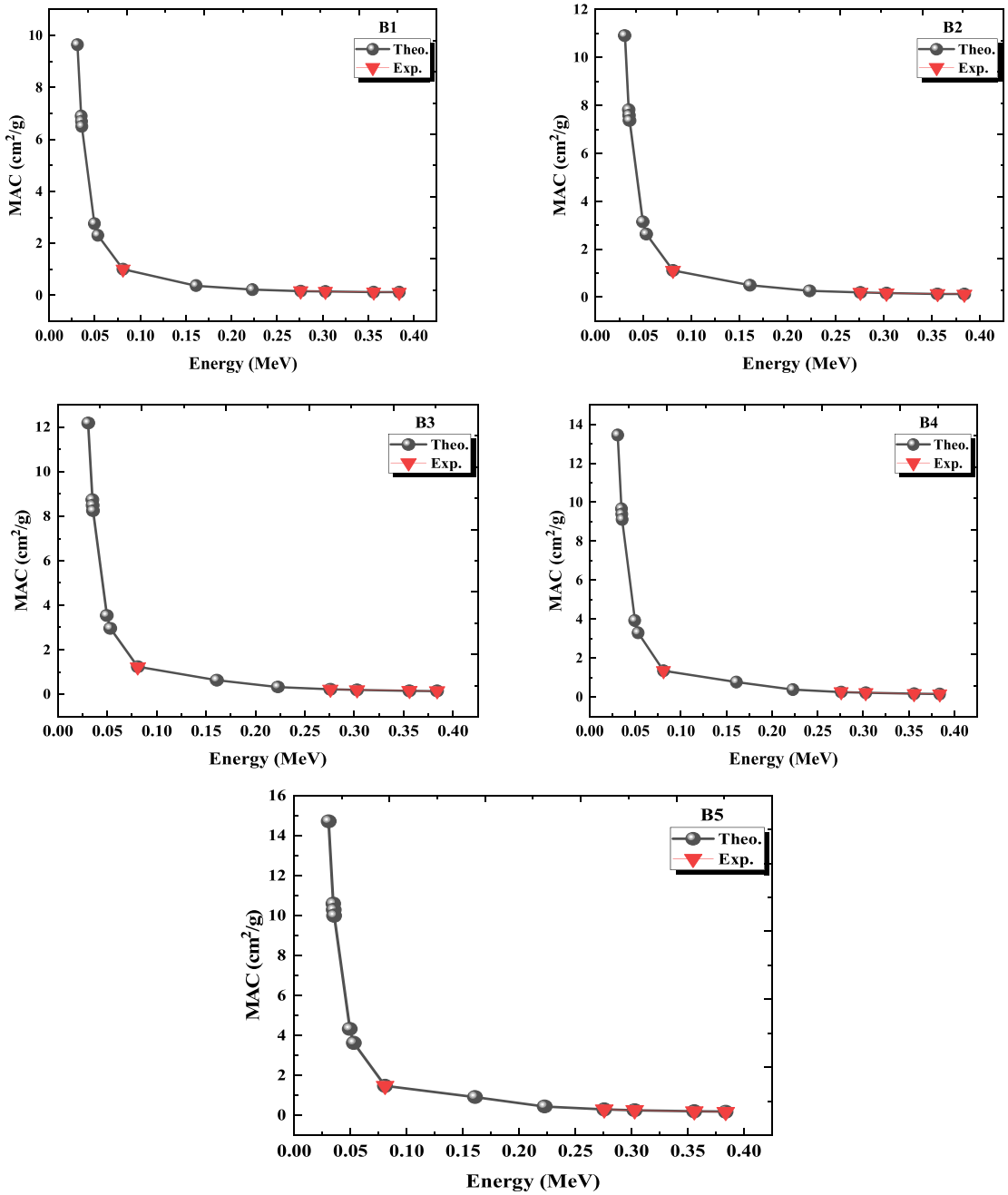

Figure 5. Variation of MAC of B1-B5 as a function of photon energy.

with photon energy. The trend of the MFP is the same as that of the HVL. The findings reveal that the investigated samples can be used in the area of γ-ray safety.

4. Conclusion

During the study, Lithium borate glass-ceramics with a composition of $40Li_2B_4O_7 + xBi_2O_3 + (55\text{-}x)\ ZrO_4 + 5CaWO_4$ (x = 10–50 wt%) have been fabricated via ordinary melt quenching route. Physical and structural characteristics as well as radiation shielding competence have been examined experimentally using an Ultra Ge detector with the ^{133}Ba (3 Ci) radioisotope source and theoretically using EpiXS software. Results showed that for sample B1which contains a minimum amount of Bi_2O_3 and maximum amount of ZrO_4, structures with large crystal particle sizes have been formed. However, the B5 structure has the largest average crystalline particle size and the structure with the smallest amount of ZrO_4 and the largest amount of Bi_2O_3 has become completely amorphous. Experimentally, density of the studied samples prepared B1-B5 samples was gradually varied between 4.70 to 5.99 g cm^{-3} for samples from B1-B5. In terms of γ-ray protection parameters, the B5 sample

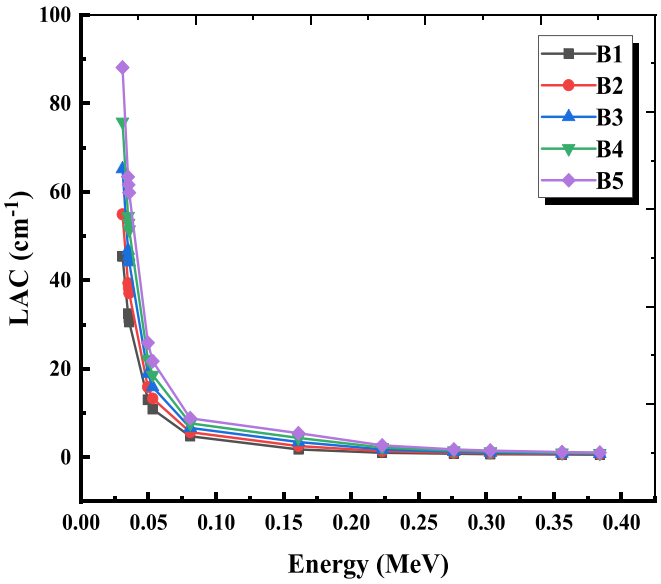

Figure 6. Variation of LAC of B1-B5 as a function of photon energy.

Table 4. Theoretical linear attenuation coefficient (LAC) of B1-B5 samples.

Energy (MeV)	B1 (Theo.)	B2 (Theo.)	B3 (Theo.)	B4 (Theo.)	B5 (Theo.)
3.08E-02	45.338	54.888	65.152	75.823	88.110
3.50E-02	32.410	39.322	46.756	54.489	63.392
3.54E-02	31.453	38.170	45.393	52.908	61.560
3.58E-02	30.535	37.064	44.085	51.392	59.802
4.96E-02	12.962	15.831	18.921	22.142	25.848
5.32E-02	10.843	13.255	15.854	18.564	21.682
8.10E-02	4.709	5.625	6.604	7.618	8.787
1.61E-01	1.729	2.526	3.405	4.347	5.421
2.23E-01	0.999	1.354	1.744	2.158	2.631
2.76E-01	0.757	0.974	1.210	1.459	1.744
3.03E-01	0.683	0.860	1.052	1.254	1.486
3.56E-01	0.583	0.709	0.844	0.985	1.147
3.84E-01	0.545	0.653	0.769	0.889	1.028

Table 5. Half value layer (HVL) of B1-B5 samples.

Energy (MeV)	B1 (HVL)	B2 (HVL)	B3 (HVL)	B4 (HVL)	B5 (HVL)
3.08E-02	0.015	0.013	0.011	0.009	0.008
3.50E-02	0.021	0.018	0.015	0.013	0.011
3.54E-02	0.022	0.018	0.015	0.013	0.011
3.58E-02	0.023	0.019	0.016	0.013	0.012
4.96E-02	0.053	0.044	0.037	0.031	0.027
5.32E-02	0.064	0.052	0.044	0.037	0.032
8.10E-02	0.147	0.123	0.105	0.091	0.079
1.61E-01	0.401	0.274	0.204	0.159	0.128
2.23E-01	0.694	0.512	0.398	0.321	0.263
2.76E-01	0.916	0.712	0.573	0.475	0.397
3.03E-01	1.014	0.806	0.659	0.553	0.467
3.56E-01	1.190	0.978	0.821	0.704	0.604
3.84E-01	1.271	1.061	0.901	0.779	0.674

with high density possessed the highest MAC values among all investigated samples. Therefore, The MAC values obey the trend: $(MAC)_{B1} < (MAC)_{B2} < (MAC)_{B3} < (MAC)_{B4} < (MAC)_{B5}$. The behavior of the LAC parameter is the same as of the MAC. In addition, the HVL arranged as; $(HVL)_{B5} > (T_{1/2})_{B4} > (T_{1/2})_{B3} > (T_{1/2})_{B2} > (T_{1/2})_{B1}$.

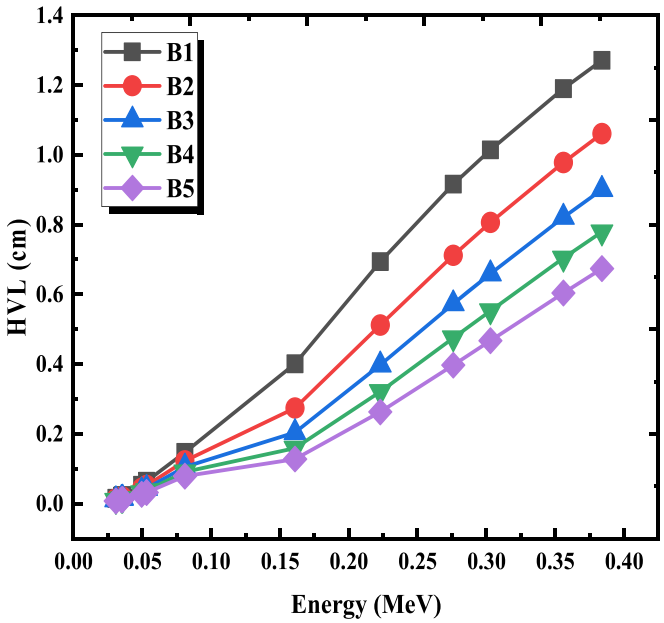

Figure 7. Variation of HVL of B1-B5 as a function of photon energy.

Table 6. Mean free path (MFP) of B1-B5 samples.

Energy (MeV)	B1 (MFP)	B2 (MFP)	B3 (MFP)	B4 (MFP)	B5 (MFP)
3.08E-02	0.022	0.018	0.015	0.013	0.011
3.50E-02	0.031	0.025	0.021	0.018	0.016
3.54E-02	0.032	0.026	0.022	0.019	0.016
3.58E-02	0.033	0.027	0.023	0.019	0.017
4.96E-02	0.077	0.063	0.053	0.045	0.039
5.32E-02	0.092	0.075	0.063	0.054	0.046
8.10E-02	0.212	0.178	0.151	0.131	0.114
1.61E-01	0.578	0.396	0.294	0.230	0.184
2.23E-01	1.001	0.739	0.574	0.463	0.380
2.76E-01	1.321	1.027	0.827	0.685	0.573
3.03E-01	1.463	1.162	0.950	0.797	0.673
3.56E-01	1.716	1.411	1.185	1.015	0.872
3.84E-01	1.834	1.530	1.300	1.124	0.973

The trend of the MFP is similar as that of the HVL. The studied glass ceramics recommended to be used as radiation protection materials.

Acknowledgments

The authors express their gratitude to Princess Nourah bint Abdulrahman, University Researchers Supporting Project (PNURSP2023R60), Princess Nourah bint Abdulrahman University, Riyadh, Saudi Arabia.

Data availability statement

All data that support the findings of this study are included within the article (and any supplementary files).

Declarations

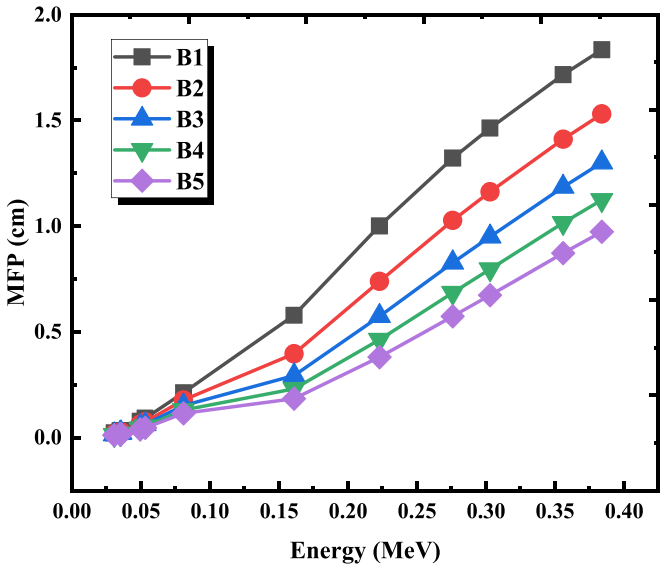

Figure 8. Variation of MFP of B1-B5 as a function of photon energy.

Compliance with ethical standards

Authors declare that this manuscript is original, has not been published before, and is not currently being considered for publication elsewhere.

Conflict of interest

The authors declare that they have no conflict of interest.

Authors contributions

NE, NAMA, BA, SS, SK, YSR: Conceptualization, Methodology, Software, Validation, Investigation, Data Curation, Writing-Review and Editing, Visualization, Supervision.

ORCID iDs

Y S Rammah https://orcid.org/0000-0003-3106-5571

References

[1] Sayyed M I, Lakshminarayana G, Kityk I V and Mahdi M A 2017 Evaluation of shielding parameters for heavy metal fluoride-based tellurite-rich glasses for gamma ray shielding applications *Radiat. Phys. Chem.* **139** 33–9
[2] Mirji R and Lobo B 2017 Radiation shielding materials: a brief review on methods, scope and significance *Proc. National Conf. on 'Advances in VLSI and Microelectronics* 27th JanuaryP.C. Jabin Science College, Huballi, India; ISBN 978-81-931806-8-6; pp. 96–100 JABINTRONICS-2017
[3] More C V, Alsayed Z, Badawi M S, Thabet A A and Pawar P P 2021 Polymeric composite materials for radiation shielding: a review *Environ. Chem. Lett.* **19** 2057–90
[4] Agar O, Sayyed M I, Akman F, Tekin H O and Kaçal M R 2019 An extensive investigation on gamma-ray shielding features of Pd/ Ag-based alloys *Nucl Eng Technol* **51** 853–9
[5] Rammah Y S, Sayyed M I, Abohaswa A S and Tekin H O 2018 FTIR, electronic polarizability and shielding parameters of B_2O_3 glasses doped with SnO_2 *Appl. Phys. A Mater. Sci. Process.* **124** 650
[6] Tekin H O, Issa S A M, Ahmed E M and Rammah Y S 2022 Lithium-fluoroborotellurite glasses: nonlinear optical, mechanical, characteristics and gamma radiation protection characteristics *Radiat. Phys. Chem.* **190** 109819
[7] Saudi H A, Zakaly H M H, Issa S A M, Tekin H O, Hessien M M, Rammah Y S and Henaish A M A 2022 Fabrication, FTIR, physical characteristics and photon shielding efficacy of CeO_2 /sand reinforced borate glasses: experimental and simulation studies *Radiat. Phys. Chem.* **191** 109837
[8] Abouhaswa A S, El-Agawany F I, Emad M, Ahmed Y S and Rammah 2022 Optical, magnetic characteristics, and nuclear radiation shielding capacity of newly synthesized barium boro-vanadate glasses: B_2O_3–BaF_2–Na_2O–V_2O_5 *Radiat. Phys. Chem.* **192** 109922

[9] Abdel-Aziz A M, Elsad R A, Ahmed E M, Rammah Y S, El-Agawany F I and Shams M S 2021 Physical, FTIR, ultrasonic, and dielectric characteristics of calcium lead-borate glasses mixed by Nd_2O_3/Er_2O_3 rare Earths: an experimental study *J. Mater. Sci., Mater. Electron.* **32** 19966–79
[10] Henaish A M A, Zakaly H M H, Saudi H A, Issa S A M, Tekin H O, Hessein M M and Rammah Y S 2022 Thermal and optical characteristics of synthesized sand/CeO_2 glasses: experimental approach *J. Electron. Mater.* **51** 2070–6
[11] Tekin H O, Kassab L R P, Shams A M, Issa C D S, Bordon E E, AltunsoyGuclu G R, da Silva Mattos O and Kilicoglu 2019 Synthesis and nuclear radiation shielding characterization of newly developed germanium oxide and bismuth oxide glasses *Ceramic International* **45** 24664–74
[12] Alajerami Y S M, Drabold D A, Mhareb M H A, Cimatu K L A, Chen G and Abushab K M 2021 Investigation of Gamma-Radiation Shielding Properties of Cadmium Bismuth Borate Glass Experimentally and by Using XCOM Program and MCNP5 Code *Physica Status Solidi (b)* **258** 2000417
[13] Ghrib T, Mhareb M H A, Sayyed M I, Alajerami Y S M, Dwaikat N, Ben Ali A and Gondal M A 2021 Structural, optical and radiation shielding properties of Zirconium–Titanium–Thallium Ternary Oxide $(0.5ZrO_2\text{-}(0.5\text{-}x)TiO_2\text{-}xTl_2O_3$ *Ceram. Int.* **47** 21837–47
[14] Mostafa A M A, Zakaly H M H, Pyshkina M, Issa S A M, Tekin H O, Sidek H A A, Matori K A and Zaid M H M 2020 Multi-objective optimization strategies for radiation shielding performance of BZBB glasses using Bi_2O_3: A FLUKA Monte Carlo code calculations *Journal of Materials Research and Technology* **9** 12335–45
[15] Mostafa A M A, Issa S A M, Zakaly H M H, Zaid M H M, Tekin H O, Matori K A, Sidek H A A and Elsaman R 2020 The influence of heavy elements on the ionizing radiation shielding efficiency and elastic properties of some tellurite glasses: theoretical investigation *Results in Physics* **19** 103496
[16] Singh J, Singh H, Sharma J, Singh T and Singh P S 2018 Fusible alloys: a potential candidate for gamma rays shield design *Prog. Nucl. Energy* **106** 387–95
[17] Issa S A M 2016 Effective atomic number and mass attenuation coefficient of PbO–BaO–B_2O_3 glass system *Radiat. Phys. Chem.* **120** 33–7
[18] Waly E-S A, Fusco M A and Bourham M A 2016 Gamma-ray mass attenuation coefficient and half value layer factor of some oxide glass shielding materials *Ann. Nucl. Energy* **96** 26–30
[19] Singh K J, Kaur S and Kaundal R S 2014 Comparative study of gamma ray shielding and some properties of PbO–SiO_2–Al_2O_3 and Bi_2O_3–SiO_2–Al_2O_3 glass systems *Radiat. Phys. Chem.* **96** 153–7
[20] Singh K J, Singh K and Singh H 2004 Comparative study of lead borate and bismuth lead borate glass systems as gamma-radiation shielding materials *Nuclear Instruments and Methods in Physics Research B* **225** 305–9
[21] Singh D, Singh K, Singh G, Manupriya, Mohan S, Arora M and Sharma G 2008 Optical and structural properties of ZnO–PbO–B_2O_3 and ZnO–PbO–B_2O_3–SiO_2 *glasses. J. Phys.: Condens. Matter.* **20** 075228
[22] Swinehart D F 1962 The Beer–Lambert law *J. Chem. Educ.*
[23] Hila F C, Asuncion-Astronomo A, Dingle C A M, Jecong J F M, Javier-Hila A M V, Gili M B Z, Balderas C V, Lopez G E P, Guillermo N R D and Amorsolo A V 2021 EpiXS: a windows-based program for photon attenuation, dosimetry, and shielding based on EPICS2017 (ENDF/B-VIII) and EPDL97 (ENDF/B-VI.8) *Radiat. Phys. Chem.* **182** 109331
[24] R.C.C. Collection, MCNPX User's Manual Version 2.4.0. Monte Carlo N-Particle Transport Code System for Multiple and High Energy Applications 2002
[25] Şakar E, E., Özpolat Ö F, Alım B, Sayyed M I and Kurudirek M 2020 Phy-X/PSD: development of a user-friendly online software for calculation of parameters relevant to radiation shielding and dosimetry *Radiat. Phys. Chem.* **166** 108496
[26] Berger M J, Hubbell J H, Seltzer S M, Chang J, Coursey J S, Sukumar R and Zucker D S 1998 XCOM: photon cross sections database *NIST Stand. Ref. Database* **8** 87–3597
[27] Al-Hadeethi Y, Sayyed M I and Rammah Y S 2020 Fabrication, optical, structural and gamma radiation shielding characterizations of GeO_2-PbO-Al_2O_3–CaO glasses *Ceram. Int.* **46** 2055–62
[28] El-Agawany F I, Tashlykov O L, Mahmoud K A and Rammah Y S 2020 The radiation-shielding properties of ternary SiO_2–SnO–SnF_2 glasses: Simulation and theoretical study *Ceram. Int.* **46** 23369–78